

**High-Average-Power Laser Optics
and Chamber Studies:
Report on Research Performed During FY01**

F. Najmabadi, M. S. Tillack and A. R. Raffray

May 1, 2002



**Fusion Division
Center for Energy Research**

University of California, San Diego
La Jolla, CA 92093-0417

ABSTRACT

This report describes the results of research performed at UC San Diego in support of the High Average Power laser program. Our research focuses on the prediction of chamber and optic response in inertial fusion energy (IFE) power plants and simulation of those phenomena through modeling and scaled experiments. Our contributions occurred in three primary topical areas: (1) Laser-induced damage to grazing-incidence metal mirrors, (2) IFE chamber dynamics and clearing following target explosions, and (3) Chamber wall materials response to pulsed loading by x-rays and high-energy ions.

Outline

1. Task 1: Final Optics Damage Studies
 - 1.1. Statement of purpose
 - 1.2. Background
 - 1.3. Progress in FY01
2. Task 2: Chamber Dynamics & Clearing
 - 2.1. Statement of Purpose
 - 2.2. Background
 - 2.3. Progress in FY01
3. Task 3: Experimental studies of laser-IFE chamber wall
 - 3.1. Statement of Purpose
 - 3.2. Background
 - 3.3. Progress in FY01

1. Task 1: Final Optics Damage Studies

1.1. Statement of purpose

Our research seeks to develop a better understanding of damage mechanisms and to demonstrate acceptable performance of grazing incidence metal mirrors (GIMM's), with an emphasis on the most critical concerns for laser IFE. Through both experimentation and modeling we will demonstrate the limitations on the operation of reflective optics for IFE chambers under prototypical environmental conditions.

1.2. Background

In any laser fusion system, the final optic for each beam is located in the direct line of sight of the exploding fusion targets. Consequently, that optic is exposed to a variety of damage threats. These include prompt neutron and gamma fluxes, x-ray and ionic emissions, and "long" time-scale threats from condensable target and chamber materials, as well as hydrodynamic pressure loads. The potential consequences include increased laser absorption, degradation of the beam quality, and reductions in the laser-induced damage threshold (LIDT).

Table 1.1 summarizes the threats and approximate goals for damage resistance. A 1% increase in absorption is likely to result in laser-induced damage to the optic as well as increased difficulty balancing the power amongst many beams. The wavefront degradation limit is chosen based on two important target illumination constraints: the spatial nonuniformity of the beam on target must be less than 1% and the spot size and position must be known to within 20 microns. As a rule of thumb, surface aberrations of the order of $\lambda/3$ ($\lambda=248$ nm for KrF) will lead to a doubling of the propagation parameter M [1], which corresponds to a doubling of the diffraction-limited spot size and a doubling of the beam divergence. The allowable wavefront distortion in the final optic depends on the allocation of wavefront distortions throughout the entire optical path as well as the margin for error. Pending further detail on the precise wavefront requirements on target, we will use the goals specified in Table 1.1.

Table 1.1. Damage threats and nominal performance goals

Final Optic Threat	Nominal Goal
Optical damage by laser	>5 J/cm ² threshold (normal to beam)
Nonuniform ablation by x-rays Nonuniform sputtering by ions	Wavefront distortion < $\lambda/3$ (~80 nm)
Defects and swelling induced by neutrons and γ -rays	Absorption loss of <1% Wavefront distortion < $\lambda/3$
Contamination by condensable materials (aerosol and dust)	Absorption loss of <1% >5 J/cm ² threshold

Two primary options for robust final optics which might survive this environment have been proposed: grazing incidence metal mirrors and refractive wedges made from a transmissive

medium such as fused silica. The two most detailed KrF laser-driven IFE conceptual power plant studies – SOMBRERO [2] and Prometheus-L [3] – both chose grazing incidence metal mirrors as their final optical element. We propose to explore this option in detail in order to establish its feasibility and to address the key issues that were identified by the designers.

Figure 1.1 shows a design of a GIMM that uses a stiff low-activation substrate (such as C or SiC composite) and a thin aluminum coating on the surface. Table 1.2 summarizes the R&D needs that were identified as important in order to establish the feasibility of this option. In our first year of research activities, we concentrated on the basic optical behavior and damage mechanisms. In our second year we propose to extend these efforts and also to begin addressing engineering development and system integration issues.

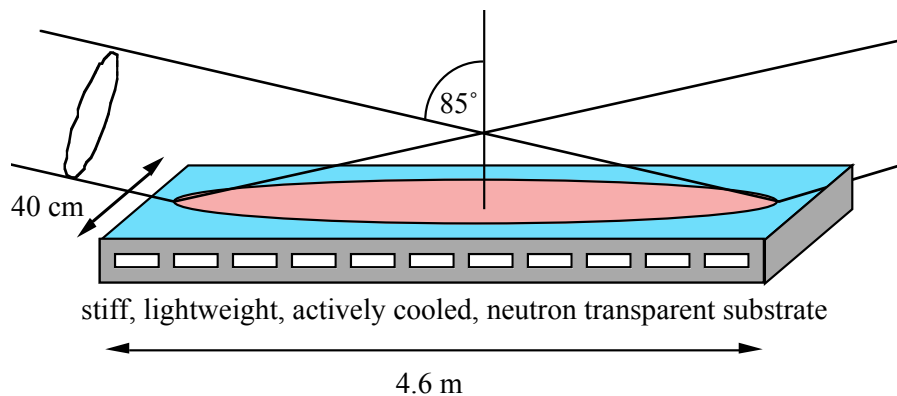


Figure 1.1. Diagram of a grazing-incidence mirror for an IFE power plant

Table 1.2. Key issues for grazing incidence mirrors in IFE [4]

1. Experimental verification of laser damage thresholds
 2. Experiments with irradiated mirrors
 3. Protection against debris and x-rays (shutters, gas jets, *etc.*)
 4. In-situ cleaning techniques
 5. Wavefront issues: beam smoothness, uniformity, shaping
 6. Large-scale manufacturing
 7. Cooling
-

1.3. Progress in FY01

During FY01 we fabricated grazing-incidence mirrors using several alloys of aluminum in order to understand the sensitivity of the damage threshold to the surface composition and morphology. Most of the mirrors were created by diamond-turning bar stock (see Fig. 1.2). A small number of samples were fabricated by sputter coating Al onto superpolished fused silica substrates. These were obtained primarily for the purpose of comparing with the diamond turned surfaces. Prior to testing, all surfaces were characterized with white light interferometry (see Fig. 1.3) and some with SEM.



Figure 1.2. Example of a diamond-turned Al mirror

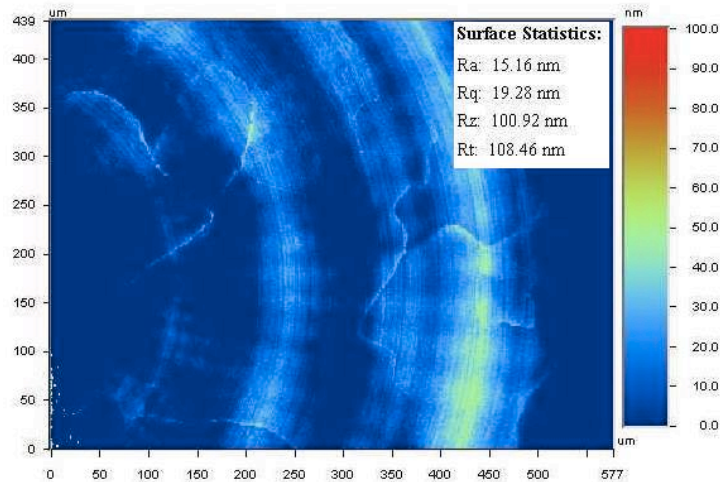


Figure 1.3. Surface analysis of a diamond-turned Al 1100 mirror

A ringdown reflectometer was constructed in order to provide a highly sensitive measurement of reflectivity (see Fig. 1.4). The reflectometer was used to characterize the surface before and after testing. In addition, in-situ measurements were made to aid in the determination of sub-critical damage (when initial degradation has occurred on the surface, but before ablation destroys the surface).

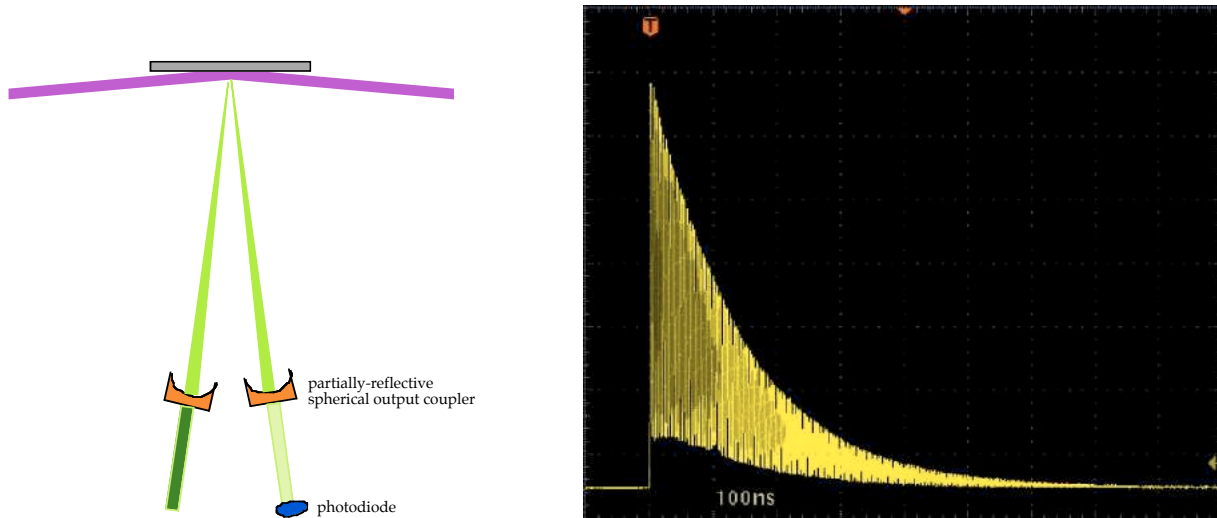


Figure 1.4. Reflectometer configuration and example oscilloscope trace

Testing was performed by passing the s-polarized light from a Nd:YAG laser through a lens before striking the Al target. The intersection of a focused cone of light with the flat Al surface placed at a shallow angle results in an ellipse of irradiation with the intensity varying along the major axis (see Fig. 1.5). In this way, each test resulted in a range of fluence levels on the surface, covering about an order of magnitude variation.

The most significant problem encountered in testing arose from the nonuniform beam emitted by the YAG laser. Careful measurements were made on the spatial intensity profile so that the fluence level was known at each point on the mirror surface (see Fig. 1.6).

Example damage photos are shown in Fig. 1.7. The fluence at which damage is initiated varies by over 2 orders of magnitude, depending on the surface. Al 6061 is highly sensitive to damage. MgSi inclusions in the surface, identified by EDX, appear to be strongly absorptive and cause explosive ejection of material at under 1 J/cm^2 normal to the beam. Al 1100 lacks these inclusions. Instead, the major surface impurity is Fe. These surfaces tend to survive up to $10\text{-}20 \text{ J/cm}^2$, depending on the number of shots. XRD analysis suggests that the ultimate mechanism for damage in this case is oxidation of these impurities. Pure Al exhibits extremely high damage threshold – as high as 160 J/cm^2 for a single shot. Cyclic stress is observed to cause defect diffusion resulting in slip planes emerging at the surface, as shown in Fig. 1.7c. This thermo-mechanical phenomenon reduces the long-term damage threshold to less than 50 J/cm^2 .

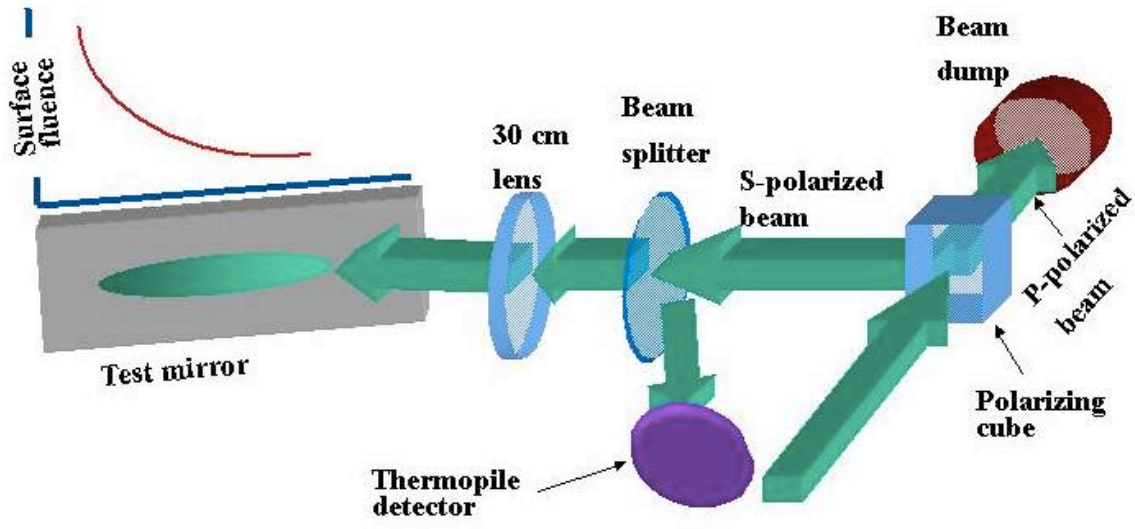


Figure 1.5. Experiment layout for damage tests

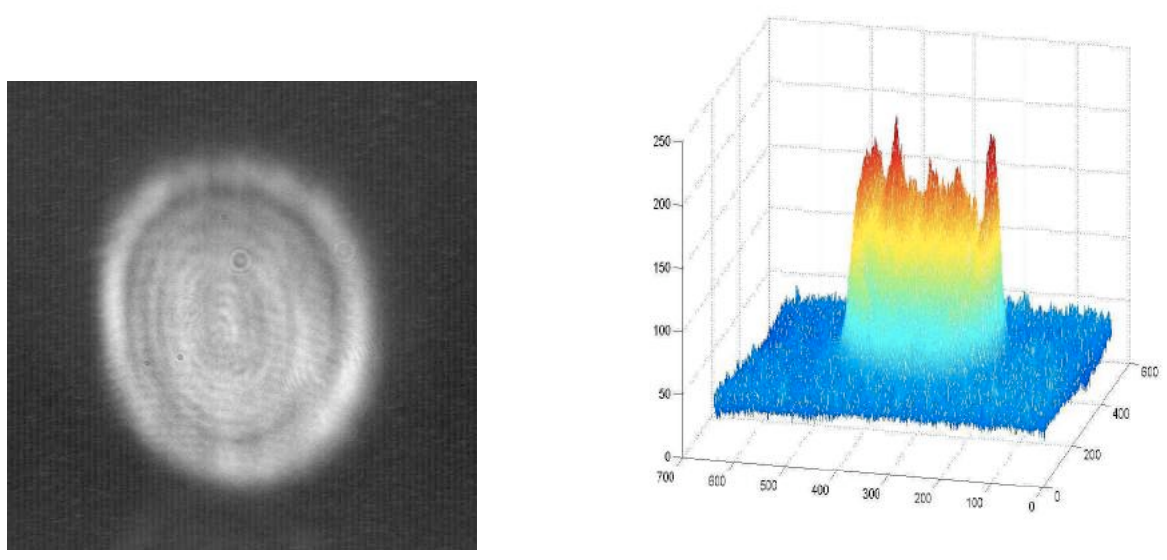
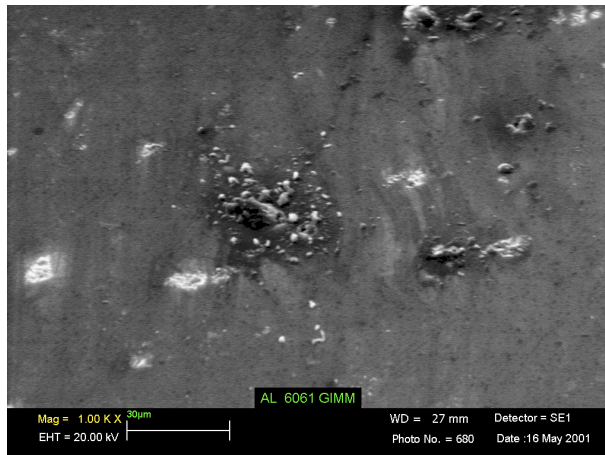
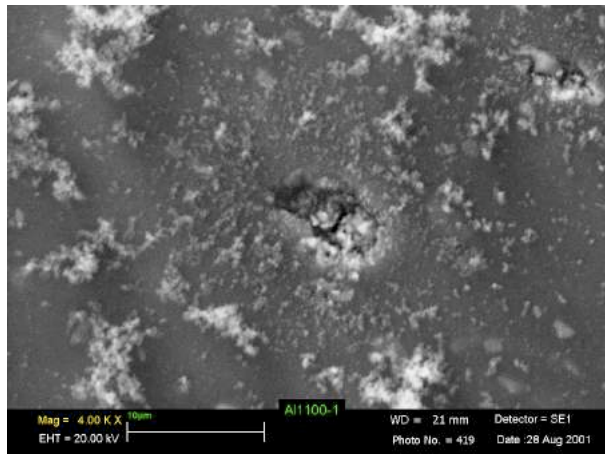


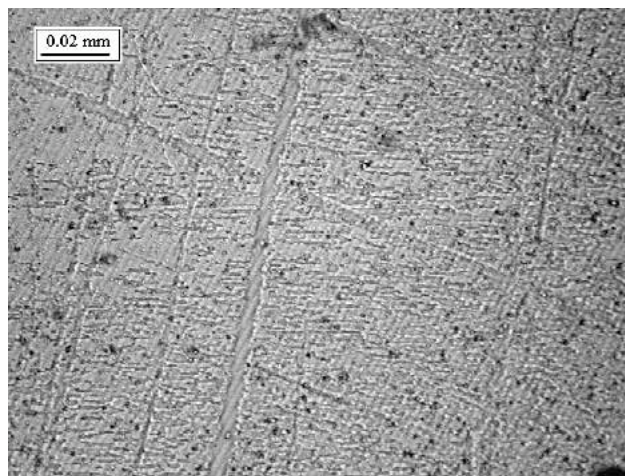
Figure 1.6. Beam intensity profile



a. Damage to Al 6061, 10 shots at 1 J/cm²



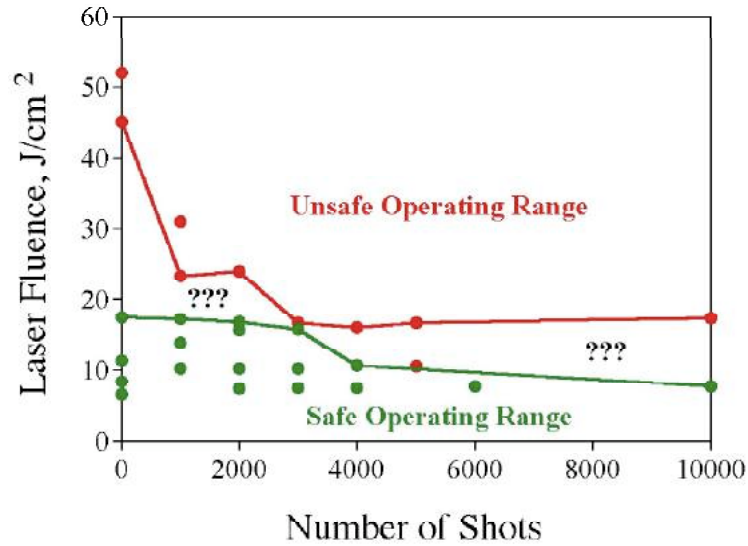
b. Damage to Al 1100, 10⁴ shots at 20 J/cm²



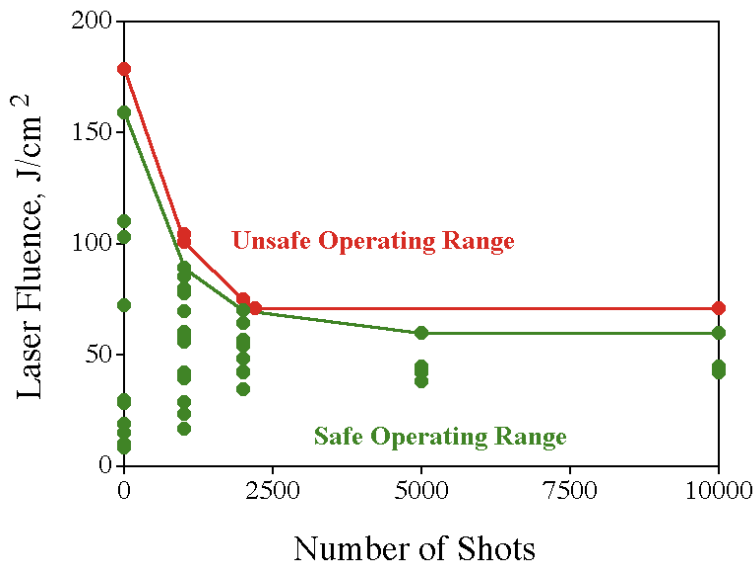
c. Damage to pure Al, 10⁴ shots at 50 J/cm²

Figure 1.7. SEM photos: a) Al 6061, b) Al 1100, c) pure Al

The full set of data is summarized in Fig. 1.8 for Al 1100 and pure Al. These charts indicate regimes of safe and unsafe operation as a function of the number of shots. The goal of operating above 5 J/cm^2 appears to be easily achievable with pure Al surfaces [5-6].



a. Al 1100



b. Pure Al

Figure 1.8. Damage plots for Al 1100 and pure Al (99.999%)

Modeling was performed to complement and help guide the experiments. The two main modeling activities were multi-layer Fresnel and Kirchhoff scattering analyses [7]. Fig. 1.9 shows a calculation of the reflectivity of Al with an oxide coating and a small amount of carbon contamination on the surface. The results identified the strong dependence of reflectivity on the coating due to enhanced optical interference at grazing angles. It also indicated that the maximum tolerable amount of carbon on the surface is of the order of 1-2 nm.

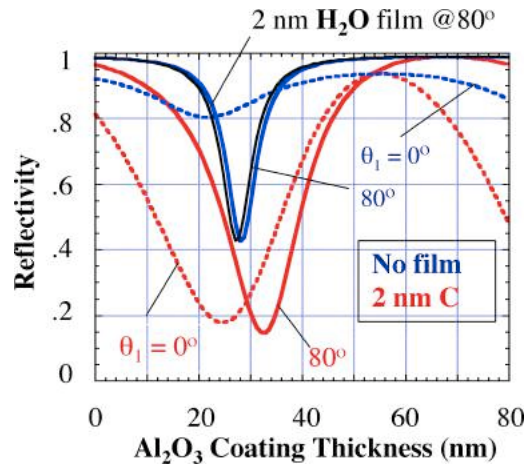


Figure 1.9 Reflectivity degradation with uniform coating and contaminant

Fig. 1.10 shows the result of a Kirchhoff scattering analysis assuming a Gaussian surface roughness distribution. This analysis was performed in order to determine limits on microscopic surface roughness that might result from surface damage accumulation. Relatively stringent limits are obtained, although operation at a shallow angle in this case helps reduce the degradation of the specularly reflected light considerably.

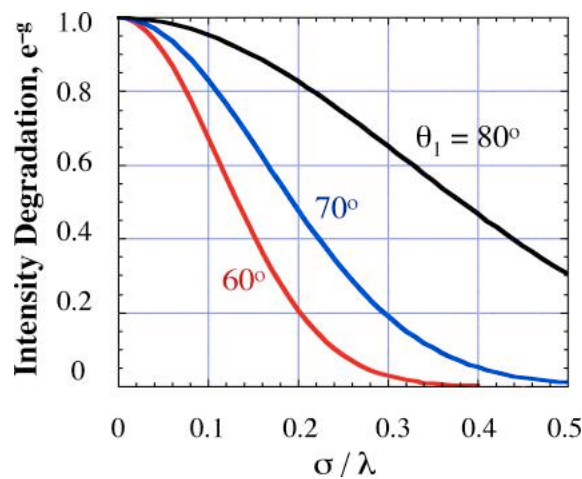


Figure 1.10 Reflectivity degradation due to surface roughening

1.4. References:

1. C. D. Orth, S. A. Payne, and W. F. Krupke, "A Diode Pumped Solid State Laser Driver for Inertial Fusion Energy," *Nuclear Fusion* 36 (1996) 75-116.
2. W. R. Meier and the W. J. Shafer Reactor Design Team. "OSIRIS and SOMBRERO Inertial Fusion Power Plant Designs – Summary, Conclusions and Recommendations," IAEA Technical Committee Meeting and Workshop on Fusion Reactor Design and Technology, 13-17 Sept. 1993.
3. L. M. Waganer, "Innovation Leads the Way to Attractive IFE Reactors – Prometheus-L & Prometheus-H," IAEA Technical Committee Meeting and Workshop on Fusion Reactor Design and Technology, 13-17 Sept. 1993.
4. R. L. Bieri and M. W. Guinan, "Grazing Incidence Metal Mirrors as the Final Elements in a Laser Driver for Inertial Confinement Fusion," *Fusion Technology* 19 (May 1991) 673-678.
5. M. S. Tillack, S. A. Payne, N. M. Ghoniem, M. R. Zaghoul and J. F. Latkowski, "Damage threats and response of final optics for laser-fusion power plants", 2nd Int. Symp. on Inertial Fusion Science and Applications, Kyoto Japan, Sept. 2001.
<http://aries.ucsd.edu/LIB/REPORT/CONF/IFSA01/tillack.pdf>
6. M. R. Zaghoul, M. S. Tillack, and T. K. Mau, "Sensitivity of Metal Mirrors to Laser-Induced Damage Under Long-Term Exposure at Shallow Angle of Incidence", 19th IEEE/NPSS SOFE, Atlantic City NJ, Jan. 21-25, 2002.
<http://aries.ucsd.edu/LIB/REPORT/CONF/SOFE01/zaghoul.pdf>
7. T. K. Mau, M. S. Tillack, and M. R. Zaghoul, "Modeling of Mirror Surface Damage Effects on Beam Propagation in a Laser-Driven IFE Power Plant", 19th IEEE/NPSS SOFE, Atlantic City NJ, Jan. 21-25, 2002.
<http://aries.ucsd.edu/LIB/REPORT/CONF/SOFE01/mau.pdf>

2. Task 2: Chamber Dynamics & Clearing

2.1. Statement of Purpose

Our research aims at developing a fully integrated computer code to model and study the IFE chamber dynamic behavior, including: the hydrodynamics; the effects of various heat sources and transfer mechanisms such as photon and ion heat deposition and chamber gas conduction, convection, and radiation; the chamber wall response and lifetime; and the cavity clearing.

2.2. Background

In a rep-rated laser-fusion facility, the pulse repetition rate is limited by the time it takes for chamber environment to return to a sufficiently quiescent and clean low-pressure state following a target explosion to allow a second shot to be initiated. Laser propagation and beam quality on the target as well target injection and tracking are impacted by the number density, temperature, mix of chamber constituents as well as fluid eddies and turbulence in the chamber.

Many physical phenomena with different time scale occur in the chamber following the target implosion. The resultant X-rays, ions and neutrons from the target travel through the chamber. Depending on the chamber constituents, the X-rays and ions can interact and deposit part of their energy in the chamber. The remaining portion of X-rays and ions arrive at the chamber wall where they deposit their energy. For the case of wetted walls, the wetting agent vaporizes and enters the chamber. In the case of a dry wall protection scheme, photons and ions will interact and affect the surface wall materials in different ways that could result in the emission of atomic (vaporization) and macroscopic particles (such as graphite or carbon composites), thereby limiting the lifetime of the wall. Also, mass loss in the form of macroscopic particles can be much larger than mass loss due to the surface vaporization. This “first pass” of target X-rays and ions through the chamber can take up to a few microseconds. At the end of this phase, the chamber environment is in a non-equilibrium phase (*e.g.*, non-uniform pressure) and a new source of material is introduced in the chamber (Figure 2.1).

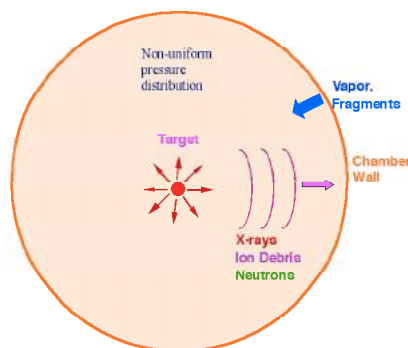


Figure 2.1. Schematic of the interaction of target energy with the chamber environment. After the “first pass” of target X-rays and ions through the chamber (a few μ s), the chamber environment is in a non-equilibrium phase (*e.g.*, non-uniform pressure) and a new source of material is introduced in the chamber.

After this phase, the chamber environment evolves mainly in the hydrodynamics time scale and a new equilibrium condition is achieved after certain time interval. The aim of the pursued research is to understand the chamber evolution and dynamic over this “longer” time scale and understand the constraints imposed by chamber dynamics on the laser driver rep-rate.

The focus of our research effort is the development of a fully integrated computer code to model and study the chamber dynamic behavior, including: the hydrodynamics; the effects of various heat sources and transfer mechanisms such as photon and ion heat deposition and chamber gas conduction, convection, and radiation; the chamber wall response and lifetime; and the cavity clearing. Since developing such a simulation capability is a major undertaking, the development of the code is envisioned in several steps of increasing sophistication, *i.e.*, the code will be developed in a modular fashion such that it can be readily and easily upgraded and more detailed physics modules added. In this fashion, the code itself can be used through its development to set priorities -- simple models can be added as modules to the code to assess the importance of different processes under different conditions. In addition, utilization of developed expertise in computational fluid dynamics allows us to focus mostly on developing and understanding relevant phenomena. Within these criteria, last year we proposed a three-year activity in development of a chamber dynamics clearing code. Code development was broken into three separate stages, each taking roughly one year of research

Stage 1 (FY01 proposal): Develop the core including the input/output interfaces, the geometry definition and the numerical solution control for transient hydrodynamics (2-D transient compressible Navier Stokes equations). Simple models for radiation and heat transport will be included. Results from BUCKY will be used as initial conditions. Boundary conditions are included through “wall-interaction” modules.

Stage 2 (FY02 proposal): Develop a detailed radiation transport package. Improve on “wall-interaction” modules based on analysis performed with stage 1 code. Implement adaptive mesh routines if necessary & extend the capability of the code to 2-D geometries with arbitrary shape.

Stage 3: Extend the code to three-dimensional problems. Incorporate improved models through analysis performed with stage 2 code as well as experimental data. At the completion of stage 3, the code upgrade will be limited to improvement in various physics modules.

Progress in Stage 1 code development (FY01 proposal) is described in the next section. We have met all milestones to date and expected to complete stage 1 code development in time.

In order to utilize diverse expertise available in the laser-IFE community, a team approach is used for this task. UCSD is responsible for the development of the code and overall management of research. Argonne National Laboratory through a subcontract with UCSD is responsible for providing models for chamber wall interaction modules describing the physics of the key mass transfer mechanisms including melting; evaporation and sublimation; sputtering and condensation. We propose for FY02 addition of INEEL that, through a subcontract with UCSD, will develop models for aerosol formation and transport to describe long term mass transport in the laser-IFE chamber. .

2.3. Progress in FY01

Development of the stage 1 code, as proposed in FY01, is on schedule and we are meeting all milestones. Code development was divided in three parts: 1) core code development (*e.g.*, numerical routines, input and output routines); 2) scoping studies to assess the relative importance of various phenomena in the chamber and to identify temporal and spatial scales; 3) development and integration simple wall interaction modules. Progress in each area is described below. In addition we had planned to use the results of a “fast-time-scale” code such as BUCKY as the initial condition for our chamber dynamics code. We have already obtained two test runs from Don Haynes of U.W. and will proceed to automate the transfer of chamber conditions from BUCKY to our chamber clearing code in the coming year.

2.3.1. Core Code Development

We have developed the core of stage 1 code. The code solves 2-D transient compressible Navier Stokes equations. Consistent with our goal of utilizing existing computational fluid dynamics capabilities and based on discussions with several specialists in the field, the code utilizes a state-of-the-art CGF solver package (after Colella, Glaz, and Ferguson) that is based on a second-order shock-capturing Godunov scheme [1,2,3]. It consists of a robust algorithm for compressible Euler equations and is second-order accurate in regions of smooth flow capturing shocks with a minimum of numerical dissipation and overshoot. A 1-D version of code with the same numerical method is evolved in parallel to the 2-D code based on the recommendation of scientists in NRL. The much faster 1-D version of code is constantly used as a test-bed for addition of new modules, for developing and testing various algorithms before implementation in the 2-D code. The code utilizes a mesh-construction routine in order to separate mesh construction from numerical algorithms. In this manner, the physical region of computation is mapped into the logical mesh of numerical solution (that is based on a 2-D rectangular mesh). Highlight of code capabilities at present are:

- 1) We have developed the core code based on single-fluid compressible Euler equations (no viscosity, no heat conduction) in 2-D rectangular grids. The code has been tested extensively in this mode.
- 2) We have developed output visualization tools for examination of code results. For example, we can produce movies of temporal evolution of chamber parameters.
- 3) We have developed mesh construction routines that translate “regular” physical domains with 2-D symmetry (*e.g.*, cylindrical symmetry) into rectangular logical mesh for computation.
- 4) A large number of problems of interest include physical domain with irregular boundary and scale-length (for example propagation of target explosion inside a chamber and a beam port). We developed a mesh construction routine that divides the physical domain into sub-domains with well-defined boundaries but with different mesh sizes. This capability (extension of the code to arbitrary 2-D geometry) was planned for stage 2 code, but given our progress in code development, was done in FY01. The necessary numerical routines are constructed, coded, and

are under test at present. This capability is essential to moving forward with mesh adaptive routines in stage 2 code.

5) Code modifications to account for viscosity and heat conduction are progressing at present. They will be coded shortly in our 1-D code in preparation for implementation in the 2-D code by March 2002.

2.3.2. Scoping Analyses

Following target explosion, X-rays and ions ionize the background gas in the chamber and deposit part of their energy in the gas (main buffer gas candidates at present is Xe). The gas cools through radiation in a fast time scale until gas temperature drop to around 1 eV. Our scoping analyses indicated that neither radiation nor conduction heat transfer mechanisms are very effective in reducing the temperature of Xe below 5,000-10,000 K. For example, Figures 2.2 shows the impact of heat conduction in the evolution of chamber gas temperature. The temperature history of a 50 mTorr Xe gas (gas pressure corresponds to 1000K) with a thermal conductivity of 0.03 W/m-K in a 5 m chamber with the wall at 1000 K is shown. It can be seen that it would take several seconds before the gas temperature drops below even 2000K. Of other noble gases, argon (with conductivity of 0.1 W/m-K) will lead to highest temperature reduction by heat conduction. Even in this case, however, it would take ~ 2 s for gas temperature to drop below 1000K. The cooling time will be even longer for cases with higher gas density.

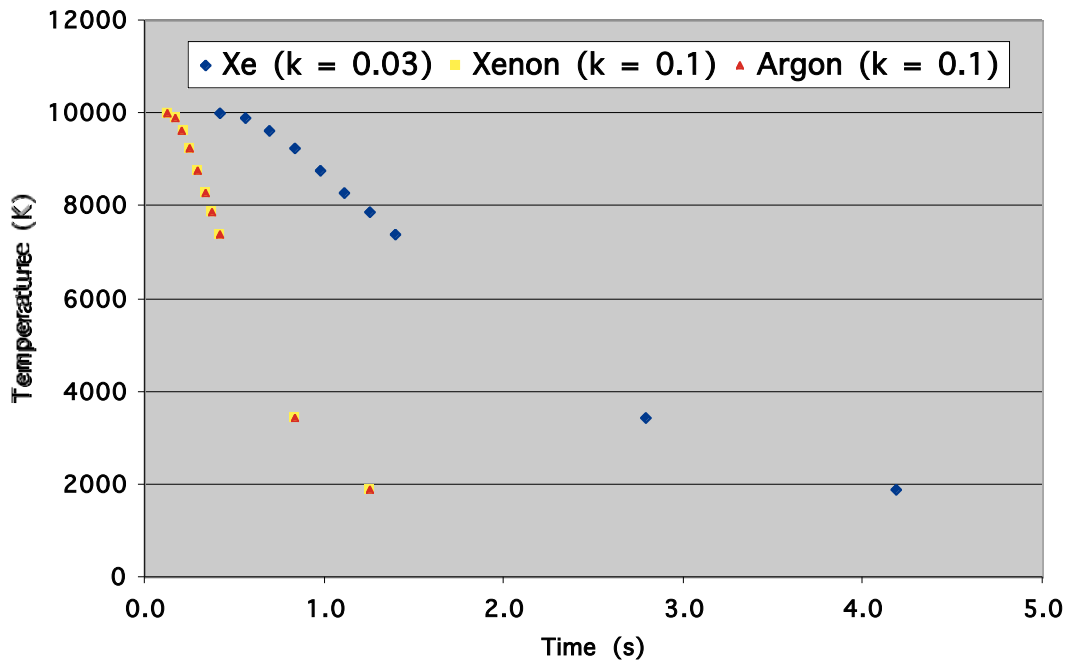


Figure 2.2. Impact of heat conduction on chamber gas temperature (50 mTorr gas in a 5 m chamber with a 1000K wall) 1) neutral Xe with $k=0.03$ W/m-K, 2) neutral Ar with $k= 0.1$ W/m-K, 3) Xe with $k=0.1$ W/m-K to simulate enhancement of heat conduction due to background electrons (residula plasma). Clearly, conduction is not sufficient to lower chamber gas temperature between shots (100-200 ms).

Scoping calculations also show that a residual plasma exists in the chamber following the fast time-scale processes. Electron conduction from this residual plasma enhances heat loss due to conduction. This effect is simulated in Fig. 2.2. by using an effective thermal conductivity of 0.1 W/m-K for Xe. Again, we conclude that conduction is not sufficient to lower chamber gas temperature between shots (100-200 ms). Similar scoping estimates indicate that radiation is not much more effective than conduction.

For convection, the indications are more positive based on local velocities and convective scale lengths. For example, Figure 2.3 shows the impact of convection in the evolution of chamber gas temperature. The temperature history of a 50 mTorr Xe gas in a 5 m chamber with the wall at 1000 K is shown. For an effective heat transfer coefficient of 0.4 W/m²-K (based on sonic velocity and a convective cell scale length of 1 m), the gas temperature reaches the wall temperature within 0.3 s. For smaller convective scale length ($h = 1 \text{ W/m}^2\text{-K}$), convective heat transfer is strong enough for the chamber gas temperature to reach equilibrium in 100 ms (corresponding with operation at 10 Hz). Clearly, convective currents and length scales of eddies are very important and this simple scoping study has justified our goal to develop a multi-dimensional code to model laser-IFE chamber dynamics.

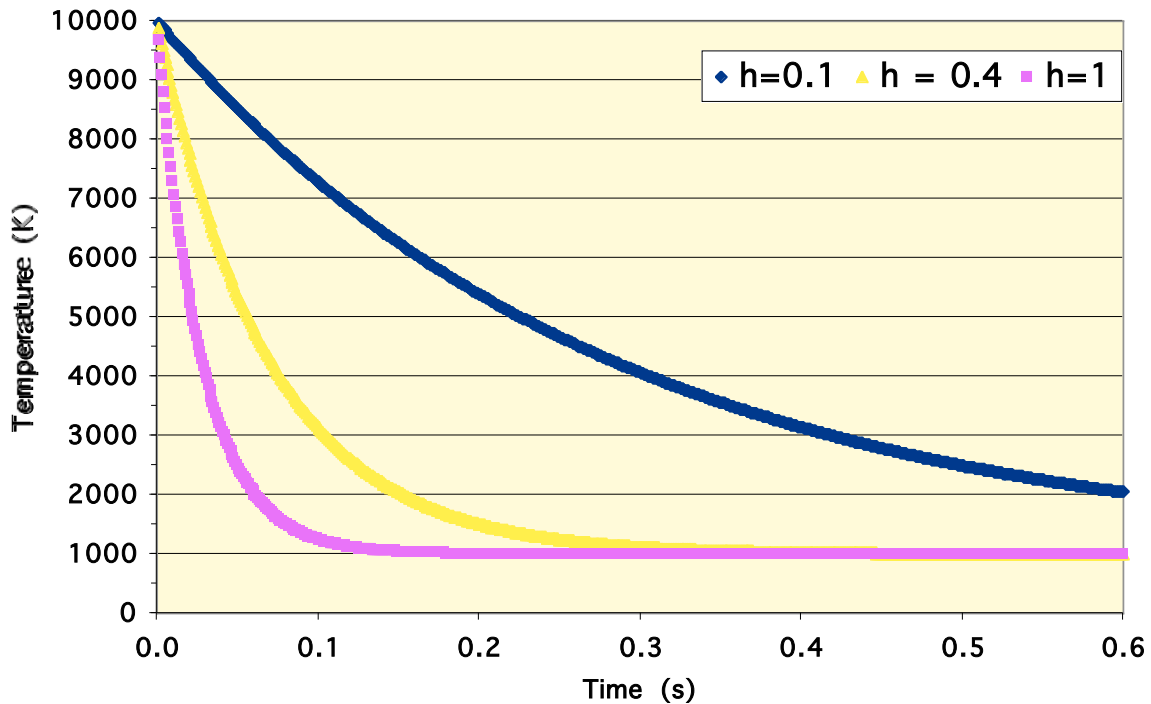


Figure 2.3. Example temperature history based on convection only from a 50 mTorr gas in a 5 m chamber to a 1000K wall for effective heat transfer coefficient, h of 0.1, 0.4 (sonic velocity and $L=1 \text{ m}$) and $1 \text{ W/m}^2\text{-K}$.

2.3.3. Wall Interaction Physics

This task is performed by Argonne National Laboratory. As stated in their recent progress report, ANL has performed preliminary parametric estimates to assess the importance of the key mass transfer processes including melting, evaporation, physical sputtering and chemical sputtering; and have developed the mathematical models and equations capturing the essential physics of these key processes. Argonne National Laboratory is to deliver in late February 2002 the full report documenting the above including details of the wall interaction module for inclusion in the stage 1 code in late February 2002.

A Simple Wall Interaction Module

We have developed at UCSD a simple wall interaction module for stage 1 code while awaiting development of more sophisticated module from Argonne National Laboratory. This module is based on a 1-D transient conduction model including evaporation, condensation and melting [4,5]. 1-D model is sufficient for this purpose as the phenomena are localized; our 2-D dynamic chamber code uses this model at each wall node. A schematic of the heat transfer processes modeled in the code is shown in Fig. 2.4. The code also calculates the mass transfer associated with the different erosion and redeposition processes.

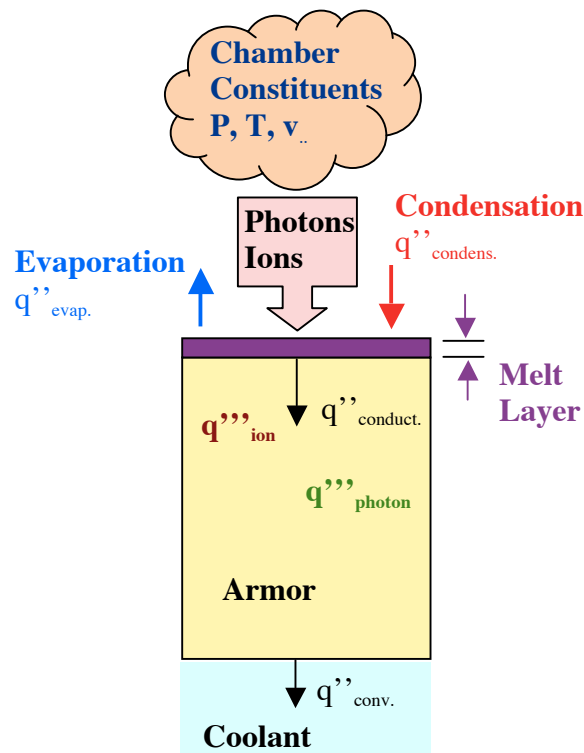


Figure 2.4. Schematic of wall interaction module illustrating the different heat transfer processes modeled in the code

2.4. References:

1. G. H. Miller and E. G. Puckett “A high-order Godunov method for multiple condensed phases,” *J. Comput. Phys.* **128** (1996) 134.
2. Marcus Day, Center for Computational Sciences and Engineering at Lawrence Berkeley National Laboratory, private communications.
3. Phil Colella, NERSC, private communications.
4. R. Raffray, and G. Federici, “RACLETTE: A Model for Evaluating the Thermal Response of Plasma Facing Components to Slow High Power Plasma Transients – Part I: Theory and Description of Model Capabilities,” *Journal of Nuclear Materials*, **244** (1997) 85-100.
5. G. Federici, and A. R. Raffray, “RACLETTE: A Model for Evaluating the Thermal Response of Plasma Facing Components to Slow High Power Plasma Transients – Part II: Analysis of ITER Plasma Facing Components,” *Journal of Nuclear Materials*, **244**, (1997) 101-130.
6. A. Hassanein, “Stability and Erosion of the Melt Layer Formed during Plasma Disruption,” *Fusion Technology* **15** (1989) 513.

3. Task 3: Experimental studies of laser-IFE chamber wall

3.1. Statement of Purpose

Our research aims at developing and fielding simulation experiments of laser-IFE chambers in order to ensure that all relevant phenomena are taken into account and benchmark modeling predictions.

3.2. Background

Investigation of laser-IFE chamber response to high-yield explosion has been mostly focused on computer modeling. It is recognized that simulation experiments are needed to ensure that all relevant phenomena are taken into account and to benchmark the calculations. While a test facility with fully prototypical conditions (including neutrons, X-rays, and debris) requires an ignited target within a factor of 10 yield as compared with a power plant chamber and with similar repetition rate, simulation experiments of most relevant phenomena can be performed with an X-ray burst of sufficient energy to produce prototypical energy density in the chamber gas ($\sim 200 \text{ kJ/m}^3$) and on the surrounding walls ($20\text{-}200 \text{ kJ/m}^2$ instantaneous and 300 kJ/m^2 integrated). As a whole, experimental study of chamber gas response to target yield is a very new field.

One of the tasks in our FY01 proposal was development of chamber simulation experiments that can be fielded in FY02. This task is completed and our findings are described below. For FY02, we propose to field such a simulation experiment.

3.3. Progress in FY01

Predictive capability of the IFE chamber response requires a detailed understanding of the response of the chamber wall as the wall response dictates the constituents of the laser IFE chamber:

1. Properties of the chamber buffer gas (e.g., type and density) are dictated by the survivability of the chamber wall,
2. Material ejected from the wall represent a major portion of material in the chamber

Most of the research to date has focused on wall mass loss due to sublimation. For a given x-ray and ion flux on the wall, temperature evolution of the wall is computed for perfectly flat wall using steady state and bulk properties for pure material. Mass loss is then estimated based on sublimation and/or melting correlations. These analyses indicate that the temperature variation mainly occurs in a thin region ($<100 \text{ }\mu\text{m}$) and large temperature gradients are limited to first few (or ten) microns. (See Figure 3.1.)

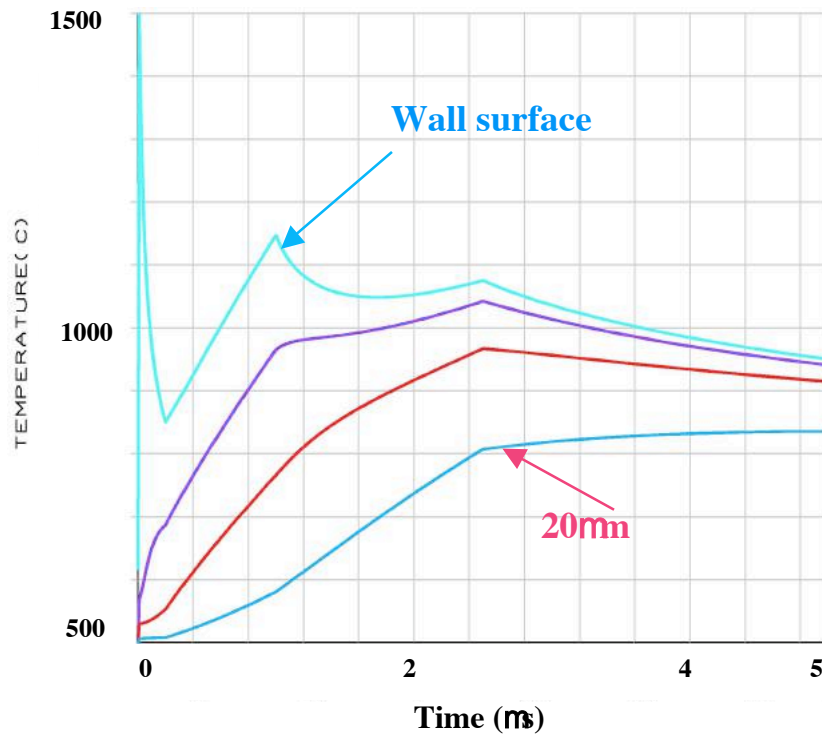


Figure 3.1. Temperature history of a flat W wall subjected to the output energy of an NRL direct drive target in 6.5-m chamber with no cover gas. Temperature evaluation on the surface and at depths of 5, 10, and 20 microns are shown.

There are a large number of uncertainties associated with this analysis and estimated material loss:

1. Surface features in a practical system are typically larger than tens of microns and impurities and contaminants can cause hot spots. As such, wall temperature estimates are highly uncertain.
2. Sublimation is extremely sensitive to material temperature and partial pressure. Accurate knowledge of wall temperature is essential in sublimation estimates. Steady-state data for sublimation rates may not be applicable to fast transients in the chamber wall. Sublimation at local hot spots (contaminants, surface morphology) may dominate. Indirect material loss due to contaminants on the surface may be important. Examples include formation of WC on the wall which has a melting point much lower than W or formation of CH on the wall that can vaporize at very low temperature.

Other phenomena that can lead to material loss include mechanical response of the wall due to thermal shock and fatigue due to differential thermal expansion. If ion flux on the wall is appreciable, sputtering and blistering also lead to mass loss. As a whole, there is a large uncertainty in calculated wall temperature and mass loss from the wall. The modeling estimates should be verified experimentally. Such experiments require real-time diagnostics of wall temperature (nanosecond or better resolution) and in-situ diagnostics of mass loss (corresponding to less than 10^{-9} m per shot). By locating the sample in a vacuum vessel, a controlled

environment can be established to measure small mass loss from the wall and to simulate wall surface contaminants.

A suite of real-time diagnostics has been identified with required precision are identified. They include:

1. **MCFOT (Multi-Color Fiber Optic Thermometry)**. MCFOT compares the thermal emission intensity at several narrow spectral bands. It has time resolutions of 0.1-1 ns and can measure temperature from ambient to ionization. Wall emissivity must be known for this diagnostics.
2. **FOTERM-S (Fiber Optic Temperature & Emissivity Radiative Measurement Self standard)**. This method compares the direct thermal emission and its self-reflection at a narrow spectral band to measure both temperature and emissivity. It has time resolutions of 0.1-1 ns and can measure temperature from ambient to ionization.
3. **QCM (Quartz Crystal Microbalance)**. QCM measures the drift in oscillation frequency of the quartz crystal. It has extreme mass sensitivity of 10^{-9} to 10^{-12} g/cm². Time resolution is < 0.1 ms (each single shot). As the quartz crystal is inexpensive, it can be detached after several shots. Composition of the ablated ejecta can be analyzed by surface examination.
4. **VISAR (Velocity Interferometer System for Any Reflector)**. VISAR measures motion of a surface. It has a time resolution of 0.1 to 1 ns and accuracy is better than 1%-2% for velocities up to 3000 m/s.
5. **RGA (residual gas analyzer)**. RGA measures constituents of chamber environment. It is reliable and precision diagnostics for measurement of long-term evolution of chamber environment.
6. **Spectrograph**. High-speed spectroscopy can provide information of the ejecta constituents (including atomic and molecular form). Sublimation and recondensation, for example, strongly depends on good knowledge of atomic and molecular form of the ejecta.

As a source with integrated and prototypical spectrum of x-rays and ions is not available, experiments should be performed in simulation facilities. Our analysis indicates that most of phenomena leading to mass loss from the wall depend on wall temperature evolution (temporal and spatial) and chamber environment; only sputtering and radiation (ion & neutron) damage effects depend on “how” the energy is delivered. Several means for delivering energy in ns time-scale are available: lasers, x-ray sources, electron beams, and ion beams.

Lasers provide a “clean” source of energy for wall simulation experiments. Irradiation of wall samples with lasers do not impose any constraint on the experimental chamber and, thus, make is relatively easy to field diagnostics. As will be discussed below, a 10-ns laser pulse can simulate temperature evolution in the wall sample that is prototypical of laser IFE chambers. Peak wall temperature and temperature gradients in the wall can be easily adjusted by controlling the laser energy and/or modification of laser pulse shape. In addition, relatively low-cost laser system can produce sufficient rep-rate to easily investigate wall response to 10^6 shots. This is specially an attractive option as existing YAG laser at UCSD can be used for this purpose.

X-rays sources are preferable to laser as the x-ray energy is deposited volumetrically in the material. However, rep-rate X-ray sources with sufficient energy for laser-IFE tests are quite expensive to build and operate.

Electron-beam sources are an attractive option. In particular, by choosing electron beam properties (such as the energy), electron beam can result in a volumetric energy deposition in the chamber wall similar to x-rays. For this reason, electron beams have been used as simulation tools in investigating material response to x-ray of nuclear weapons. An electron beam facility with the required energy and rep-rate, however, will cost over \$1M.

Ion sources are considerably more expensive than electron beams but they would provide additional data, as the primary energy release channel in direct-drive capsules is the ion channel. The existing RHEPP facility at Sandia has been used to study wall response. The drawback of this facility is its low rep-rate. In addition, special diagnostics has to be fielded on RHEPP to measure temperature evolution of sample in real time (see Task 4).

Overall, our conclusion is that laser provides the most flexible and low-cost option to investigate laser-IFE chamber wall response. Similar simulation experiments (but at low rep-rate, with small number of shots, and smaller suite of diagnostics) can be fielded in RHEPP facility. The combination of two efforts provides a large body of experimental database for laser-IFE wall research. In particular, comparison of experimental results from a laser facility with similar experiments performed in RHEPP will underline if the wall mass loss mechanism is mainly due to temperature evolution and/or other effects can be important.

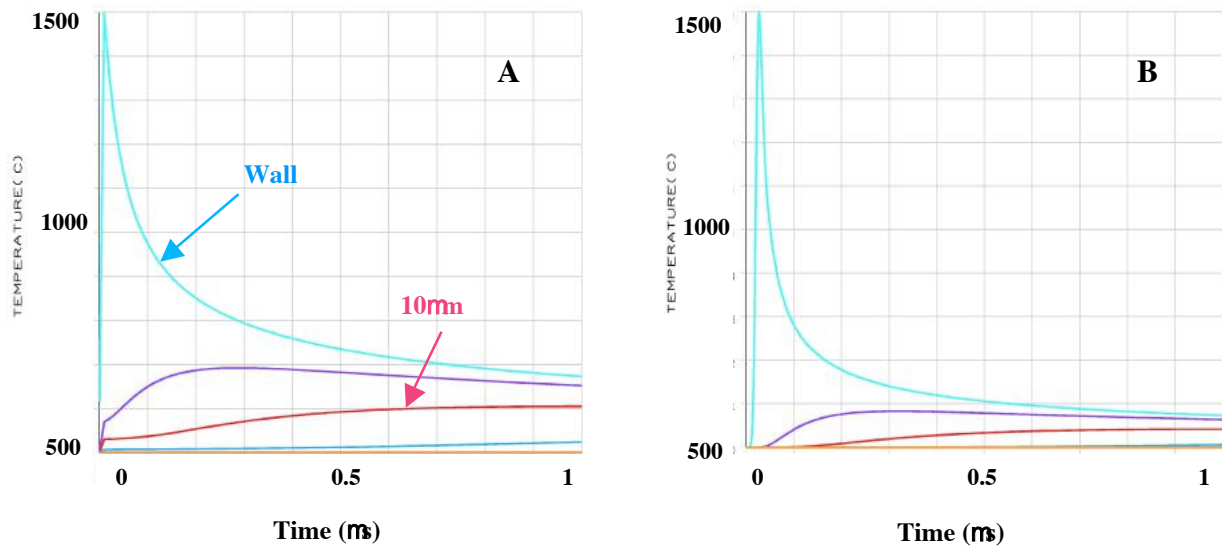


Figure 3.2. Temperature history in a tungsten flat wall subjected to a) NRL direct-drive target x-ray channel and b) a 10 ns Gaussian laser pulse. Only the laser energy is adjusted such that similar peak wall temperature (~1500 C) is achieved in the simulation experiments.

Our program has a 2 J, 10 Hz YAG:Nd laser. We have performed simulations to see if such a laser is suitable for chamber wall experiments. Because of vast difference in time-scale of x-ray and ion-energy deposition on the chamber wall, we have considered each of the two energy channel separately. Figure 3.2a shows that response of a flat tungsten wall subjected to the output x-ray energy of an NRL direct drive target in 6.5-m chamber with no cover gas. Temperature evaluation on the surface and at depths of 5, 10, and 20 microns are shown. Figure

3.2b shows that response of a similar W wall to a 10 ns Gaussian laser pulse (typical pulse from a YAG:Nd laser). Only the laser energy is adjusted such that similar peak wall temperature (~1500 C) is achieved in the simulation experiments. This simulation shows that similar temperature profiles and gradients (both temporal and spatial) can be simulated with a laser pulse. Changing laser energy and/or modifying the laser pulse shape can easily adjust peak wall temperature and wall temperature gradients.

Our simulations also indicate that the wall temperature history due to both ion and x-rays produced by the NRL direct-drive target (Fig. 3.1) can be simulated using three lasers pulses: a 10 ns laser pulse to simulate the X-ray effects and two μ s-duration laser pulses with much smaller energy (that can be produced by an expensive CO₂, for example).

In summary, our work indicate that:

- a) There is a large uncertainty in estimated material loss from chamber wall,
- b) Real-time and fast diagnostics is essential to simulation experiments,
- c) A set of diagnostics has been identified.
- d) A simulation facility using lasers as a energy source can simulate temperature evolution of laser IFE chamber wall,
- e) Combination of simulation experiments in a laser facility and fielding diagnostics on RHEPP ion beam facility will provide a rich data base for laser-IFE chamber wall response.

We have also performed conceptual design for MCFOT and FOTERMS-S. QCM and RGA diagnostics are available commercially and quotes from vendors have been obtained. Preliminary design of a sample holder that can operate at high temperatures is under way.